

TYPE IA SUPERNOVA DISTANCES AT REDSHIFT > 1.5 FROM THE HUBBLE SPACE TELESCOPE MULTI-CYCLE TREASURY PROGRAMS: THE EARLY EXPANSION RATE

ADAM G. RIESS^{1,2}, STEVEN A. RODNEY³, DANIEL M. SCOLNIC⁴, DANIEL L. SHAFER¹, LOUIS-GREGORY STROELGER², HENRY C. FERGUSON², MARC POSTMAN², OR GRAUR^{5,6,7}, DAN MAOZ⁸, SAURABH W. JHA⁹, BAHRAM MOBASHER¹⁰, STEFANO CASERTANO², BRIAN HAYDEN^{11,12}, ALBERTO MOLINO¹³, JENS HJORTH¹⁴, PETER M. GARNAVICH¹⁵, DAVID O. JONES¹, ROBERT P. KIRSHNER⁵, ANTON M. KOEKEMOER², NORMAN A. GROGIN², GABRIEL BRAMMER², SHOUBANEH HEMMATI¹⁶, MARK DICKINSON¹⁷, PETER M. CHALLIS⁵, SCHUYLER WOLFF¹, KELSEY I. CLUBB¹⁸, ALEXEI V. FILIPPENKO^{18,19}, HOOSHANG NAYYERI²⁰, VIVIAN U^{10,20,21}, DAVID C. KOO²², SANDRA M. FABER²², DALE KOCEVSKI²³, LARRY BRADLEY², AND DAN COE²

Draft version October 4, 2017

ABSTRACT

We present an analysis of 15 Type Ia supernovae (SNe Ia) at redshift $z > 1$ (9 at $1.5 < z < 2.3$) recently discovered in the CANDELS and CLASH Multi-Cycle Treasury programs using WFC3 on the *Hubble Space Telescope*. We combine these SNe Ia with a new compilation of ~ 1050 SNe Ia, jointly calibrated and corrected for simulated survey biases to produce accurate distance measurements. We present unbiased constraints on the expansion rate at six redshifts in the range $0.07 < z < 1.5$ based only on this combined SN Ia sample. The added leverage of our new sample at $z > 1.5$ leads to a factor of ~ 3 improvement in the determination of the expansion rate at $z = 1.5$, reducing its uncertainty to $\sim 20\%$, a measurement of $H(z = 1.5)/H_0 = 2.67^{+0.83}_{-0.52}$. We then demonstrate that these six measurements alone provide a nearly identical characterization of dark energy as the full SN sample, making them an efficient compression of the SN Ia data. The new sample of SNe Ia at $z > 1.5$ usefully distinguishes between alternative cosmological models and unmodeled evolution of the SN Ia distance indicators, placing empirical limits on the latter. Finally, employing a realistic simulation of a potential *WFIRST* SN survey observing strategy, we forecast optimistic future constraints on the expansion rate from SNe Ia.

Keywords: cosmology: observations — methods: observational — supernovae: general

ariess@stsci.edu

¹ Department of Physics and Astronomy, The Johns Hopkins University, 3400 North Charles Street, Baltimore, MD 21218, USA

² Space Telescope Science Institute, 3700 San Martin Drive, Baltimore, MD 21218, USA

³ Department of Physics and Astronomy, University of South Carolina, 712 Main Street, Columbia, SC 29208, USA

⁴ Kavli Institute for Cosmological Physics, University of Chicago, 5640 South Ellis Avenue, Chicago, IL 60637

⁵ Harvard-Smithsonian Center for Astrophysics, 60 Garden Street, Cambridge, MA 02138, USA

⁶ Department of Astrophysics, American Museum of Natural History, Central Park West and 79th Street, New York, NY 10024, USA

⁷ NSF Astronomy and Astrophysics Postdoctoral Fellow

⁸ School of Physics and Astronomy, Tel Aviv University, Tel Aviv 69978, Israel

⁹ Department of Physics and Astronomy, Rutgers, The State University of New Jersey, Piscataway, NJ 08854, USA

¹⁰ Department of Physics and Astronomy, University of California, 900 University Avenue, Riverside, CA 92521, USA

¹¹ Lawrence Berkeley National Laboratory, Berkeley, CA 94720, USA

¹² Department of Physics, University of California, Berkeley, CA 94720, USA

¹³ Instituto de Astronomia, Geofísica e Ciências Atmosféricas, Universidade de São Paulo, Cidade Universitária, 05508-090, São Paulo, Brazil

¹⁴ Dark Cosmology Centre, Niels Bohr Institute, University of Copenhagen, Juliane Maries Vej 30, DK-2100 Copenhagen, Denmark

¹⁵ Department of Physics, University of Notre Dame, Notre Dame, IN 46556, USA

¹⁶ Infrared Processing and Analysis Center, California Institute of Technology, Pasadena, CA 91125, USA

¹⁷ National Optical Astronomy Observatory, 950 North Cherry Avenue, Tucson, AZ 85719, USA

¹⁸ Department of Astronomy, University of California, Berke-

ley, CA 94720-3411, USA

¹⁹ Miller Senior Fellow, Miller Institute for Basic Research in Science, University of California, Berkeley, CA 94720, USA

²⁰ Department of Physics and Astronomy, University of California, Irvine, CA 92697, USA

²¹ University of California Chancellor's Postdoctoral Fellow

²² Department of Astronomy and Astrophysics, University of California, Santa Cruz, CA 95064, USA

²³ Colby College, 4000 Mayflower Hill Drive, Waterville, ME 04901, USA

1. INTRODUCTION

Type Ia supernovae (SNe Ia) at redshift $z > 1$ offer unique leverage on investigations relating to the nature of their progenitors, their accuracy as distance indicators, and the parameters of the cosmological model. Unfortunately, ground-based facilities are extremely challenged to produce reliable discoveries of SNe Ia at $z > 1$, a task demanding significant and repeatable detections and robust classifications at $I \sim 26$ mag.

Thus, for the past two decades, the *Hubble Space Telescope* (*HST*) has offered the best perch from which to harvest these objects, with the rate of collection limited only by its relatively modest field of view. The first robust, multi-object sample of SNe Ia at $z > 1$ came from searching the GOODS fields with the *HST* Advanced Camera for Surveys (ACS) and its z -band filter, with crucial near-infrared follow-up observations of the rest-frame optical light obtained using NICMOS and confirming spectroscopy from the ACS grism. The first sample of 7 SNe Ia at $z > 1.25$ provided a crucial check that dimming from astrophysical effects was not mimicking cosmic acceleration (Riess et al. 2004). A follow-up program increased the sample of reliable SNe Ia at $z > 1$ to 18 (Riess et al. 2007) followed by another 12 from targeting cluster fields (Suzuki et al. 2012). This sample of ~ 30 successfully extended the SN Ia measurement of expansion to the matter-dominated era to break degeneracies between dark energy and dark matter.

Still, clues available only at $z > 1.5$ beckoned. Owing to the red-limit of *HST* CCDs and the roughly Gyr delay between progenitor formation and SN Ia explosion (Rodney et al. 2014), only ~ 3 moderately constrained SNe Ia at $z > 1.5$ were previously discovered with *HST*: SN 1997ff at $z = 1.755$, SN 2003ak at $z = 1.551$, and SCP0401 at $z = 1.713$ (Gilliland et al. 1999; Riess et al. 2001; Riess et al. 2004; Rubin et al. 2013). An effective program to find SNe Ia at $z > 1.5$ required WFC3-IR, the first wide-area (greater than an arcminute) infrared HgCdTe detector on *HST*, installed in 2009, which extended the red cutoff to $1.6 \mu\text{m}$. Two of the initial three Multi-Cycle Treasury (MCT) programs with WFC3, CANDELS (PI: Faber and Ferguson, Grogin et al. 2011; Koekemoer et al. 2011) and CLASH (PI: Postman, Postman et al. 2012) were selected to enable the discovery of SNe Ia at $z > 1.5$ with an additional program of coordinated SN follow-up observations (PI: Riess, Rodney et al. 2014; Graur et al. 2014). These MCT programs were three-year extragalactic imaging campaigns initiated in *HST* Cycle 18, beginning October 2010. Both MCT programs employed ACS and WFC3-IR with cadences of ~ 50 days between epochs, chosen to match the risetime of SNe Ia time-dilated to $1.5 < z < 2.0$. Rodney et al. (2014, hereafter R14) comprehensively described the SN search component of the CANDELS program and measured the volumetric SN Ia rate from the complete CANDELS sample of 65 SNe out to $z = 2.5$. Graur et al. (2014, hereafter G14) presented the SN Ia rates analysis from the CLASH program, using a sample of 27 SNe detected in the *HST* parallel fields ($\sim 6'$ from the galaxy clusters that make up the primary targets for CLASH). For full details of the survey design and observations, we refer the reader to R14 and G14.

These programs together identified 15 SNe Ia at $z > 1$,

9 of which (7 at $z > 1.5$) are sufficiently well-measured to derive reliable distance estimates. Detailed studies of the first two such events were presented by Rodney et al. (2012) and Jones et al. (2013), and a novel approach to SN classification via medium-band infrared imaging was presented for two others by Rodney et al. (2015).

Here for the first time we derive a set of distance estimates for this sample calibrated for a joint cosmological analysis with a compilation of SNe Ia from previous surveys (Scolnic et al. 2017, in prep). The most significant augmentation of the extant SN Ia sample is the set of SN Ia distances presented here at $z > 1.5$, which usefully extends the SN-based determination of the expansion rate of the universe to a higher redshift, $z \approx 1.5$, than previously possible. In Section 2, we present details of the SN sample, and in Section 3, we present constraints on the scale-free expansion history and carry out some related investigations. We summarize our conclusions in Section 4.

2. SN IA SAMPLE

From the total set of 92 CANDELS and CLASH SNe, we have identified 15 as likely SNe Ia at $z > 1$ with sufficient confidence for use as distance indicators. We present the coordinates of these objects in Table 1, their redshifts and classifications in Table 2, the properties of their host galaxies in Table 3, and their distance-related parameters in Table 4. For inclusion in this subset, we require at least enough samplings of the light and color curves to exceed the number of free parameters in the light-curve fit. This effectively means that we require a minimum of four independent observation epochs, providing at least a modicum of constraint on the light-curve shape. We also require that the first epoch with $> 3\sigma$ detection must be no more than 10 days after the peak of the light curve in the rest-frame B band, consistent with the requirements used by Riess et al. (1996) and Riess et al. (2007). Finally, we require that at least one of the epochs includes WFC3-IR observations in both the $F125W$ and $F160W$ bands, which provide a measurement of the SN color at rest-frame optical wavelengths for $1 < z < 2.5$.

For the cosmological analysis presented here, we further subdivide this sample into three confidence categories: *gold*, *silver*, and *bronze*, following the convention of Strolger et al. (2004), Riess et al. (2004), and Riess et al. (2007). The gold sample comprises those SNe with compelling classifications as Type Ia, while the silver label indicates a “very likely” Type Ia classification, and the bronze objects are those that are probably Type Ia, but have some nonnegligible probability of misclassification.

As detailed by R14 and G14, the classifications of these SNe at $z > 1$ sometimes rely on photometric evidence. Spectra are available for 6 of the 15 SNe Ia at $z > 1$ (3 at $z > 1.5$), while two others use medium bands to measure the strength of SN Ia spectral features. This mixture of classification methods is necessitated by the difficulty of achieving a purely spectroscopic classification for such high-redshift SNe (see, e.g., Rodney et al. 2012; Frederiksen et al. 2012; Rubin et al. 2013; Jones et al. 2013). Photometric classification of these SNe was performed using

Table 1
SNe Ia from CANDELS + CLASH at $z > 1$

SN ID	Nickname	Survey	Field	α (J2000)	δ (J2000)
CLA10Cal	Caligula	CLASH	Abell 383 IR par	02:48:25.74	-03:33:08.8
CLF11Ves	Vespasian	CLASH	MACS2129 ACS par	21:29:42.60	-07:41:47.7
CLH11Tra	Trajan	CLASH	MS2137 ACS par	21:39:46.05	-23:38:34.8
CLP12Get	Geta	CLASH	RXJ2129 IR par	21:29:23.89	+00:08:24.8
COS12Car	Carter	CANDELS	COSMOS	10:00:14.72	+02:11:32.6
EGS11Oba	Obama	CANDELS	EGS	14:20:32.66	+53:02:48.2
EGS13Rut	Rutledge	CANDELS	EGS	14:20:48.11	+53:04:22.1
GND12Col	Colfax	CANDELS	GOODS-N Deep	12:36:37.58	+62:18:33.1
GND13Cam	Camille	CANDELS	GOODS-N Deep	12:37:07.37	+62:10:26.9
GND13Gar	Garner	CANDELS	GOODS-N Deep	12:36:40.81	+62:11:14.2
GND13Jay	Jay	CANDELS	GOODS-N Deep	12:36:41.38	+62:11:30.1
GND13Sto	Stone	CANDELS	GOODS-N Deep	12:37:16.77	+62:16:41.4
GSD10Pri	Primo	CANDELS	GOODS-S Deep	03:32:38.01	-27:46:39.1
GSD11Was	Washington	CANDELS	GOODS-S Deep	03:32:20.85	-27:49:41.5
UDS10Wil	Wilson	CANDELS	UDS	02:17:46.33	-05:15:24.0

Table 2
Final Redshifts and Classifications

SN ID	Redshift ^a	Redshift Source ^b	P (Ia) ^c	Supporting Evidence ^d	Confidence ^e	Primary Reference ^f
CLA10Cal	1.800±0.1	phot- z	0.95	...	bronze	Graur et al. (2014)
CLF11Ves	1.206±0.007	spec- z (<i>HST</i> +G800L)	>0.99	spec, early-type host	gold	Graur et al. (2014)
CLH11Tra	1.520±0.04 ^g	phot- z	>0.99	early-type host	gold	Graur et al. (2014)
CLP12Get	1.700±0.04	phot- z	>0.99	early-type host	gold	Graur et al. (2014)
COS12Car	1.540±0.04	SN spec- z (<i>HST</i> +G141)	>0.99	spec	gold	Rodney et al. (2014)
EGS11Oba	1.409±0.002	spec- z (Keck+LRIS,DEIMOS)	0.9	...	bronze	Rodney et al. (2014)
EGS13Rut	1.614±0.005	spec- z (<i>HST</i> +G141, single line)	>0.99	...	silver	Rodney et al. (2014)
GND12Col	2.260 ^{+0.02} _{-0.10}	phot- z	>0.99	med. band	gold	Rodney et al. (2015)
GND13Cam	1.222±0.002	spec- z (AGHAST, <i>HST</i> +G141)	>0.99	...	silver	Rodney et al. (2014)
GND13Gar	1.070±0.02	SN spec- z (<i>HST</i> +G800L)	>0.99	spec	gold	Rodney et al. (2014)
GND13Jay	1.030±0.01	spec- z (AGHAST, <i>HST</i> +G141)	>0.99	...	silver	Rodney et al. (2014)
GND13Sto	1.800±0.02	spec- z	>0.99	med. band	gold	Rodney et al. (2015)
GSD10Pri	1.550±0.0001	spec- z	>0.99	spec	gold	Rodney et al. (2012)
GSD11Was	1.330±0.02	spec- z (<i>HST</i> +G141)	>0.99	spec	gold	Rodney et al. (2014)
UDS10Wil	1.914±0.001	spec- z	>0.99	spec	gold	Jones et al. (2013)

^a Final composite redshift, incorporating all evidence from SN and host.

^b All phot- z and spec- z redshifts are principally constrained by the host galaxy, except where a SN spec- z is noted.

^c Classification probability from the SN light curve, including host redshift priors, using STARDUST (R14).

^d Additional factors influencing the classification confidence. “spec”: SN spectrum; “med. band”: pseudocolors from medium-band infrared imaging; “early-type host”: host galaxy is identified as an early-type galaxy, unlikely to host core-collapse SNe.

^e Confidence in the Type Ia SN classification.

^f Primary reference for further information on discovery, redshift, and classification.

^g Revised from Graur et al. (2014)

STARDUST²⁴, a Bayesian algorithm employing a comparison of multi-band light curves against 43 template-based models representing Type Ia and core-collapse SNe (R14). For inclusion in the gold and silver samples, we require a Type Ia classification probability P (Ia) > 0.99; the two objects with $0.9 < P$ (Ia) < 0.99 were relegated to the bronze sample.

The gold objects are further distinguished by having at least one piece of corroborating evidence to support the Type Ia classification. For 6 objects, we have a spectroscopic observation that is well-matched by a SN Ia spectral template, presented by R14 and G14. Two more SNe have medium-band infrared imaging that provides evidence for Type Ia *spectral features* in medium-band minus broad-band pseudocolors (Rodney et al. 2015). Finally, three of the gold sample SNe have a host galaxy

that is classified as “early type” based on morphology and colors, indicating an old stellar population that would be unlikely to host a core-collapse SN (Riess et al. 2001).

We discard the 2 bronze SNe whose classification is too uncertain and proceed with the analysis of the remaining 13 gold and silver SNe at $z > 1$ (8 at $z > 1.5$) from the CANDELS and CLASH programs. Assuming the 3 silver SNe in the sample are Type Ia with 99% confidence, there is a $\sim 97\%$ chance that all of the SNe in the cosmological analysis are Type Ia. We combine this set (hereafter, the MCT set) with a uniformly calibrated compilation of ~ 1050 spectroscopically classified SNe Ia, the Pantheon compilation (Scolnic et al. 2017). This compilation includes SNe from the Harvard-Smithsonian Center for Astrophysics SN surveys (CfA, Hicken et al. 2009), the Carnegie Supernova Project (CSP, Stritzinger et al. 2011), the Sloan Digital Sky Survey (SDSS, Kessler

²⁴ STARDUST: Supernova Taxonomy And Redshift Determination Using SNANA Templates

Table 3
SN Host Galaxy Data

SN ID	Host α (J2000)	Host δ (J2000)	Host Redshift ^a	Morphology	Star Formation	Redshift Source
CLA10Cal	02:48:25.74	-03:33:08.8	1.8±0.1	spheroid/disk	active	phot- <i>z</i>
CLF11Ves	21:29:42.62	-07:41:47.5	1.206±0.007	spheroid	passive	<i>HST</i> +ACS
CLH11Tra	21:39:46.04	-23:38:34.6	1.52±0.04	spheroid	passive	phot- <i>z</i>
CLP12Get	21:29:23.92	+00:08:23.8	1.70±0.04	spheroid	passive	phot- <i>z</i>
COS12Car ^b	10:00:14.72	+02:11:32.6	...	undetected	undetected	...
EGS11Oba	14:20:32.67	+53:02:48.1	1.409±0.002	disk/irregular	active	Keck+LRIS
EGS13Rut	14:20:48.11	+53:04:22.1	1.614±0.005	disk	active	<i>HST</i> +WFC3
GND12Col	12:36:37.51	+62:18:32.6	2.260 ^{+0.02} _{-0.10}	spheroid	active	phot- <i>z</i>
GND13Cam	12:37:07.38	+62:10:27.2	1.222±0.002	spheroid/disk	starburst	<i>HST</i> +WFC3
GND13Gar	12:36:40.80	+62:11:14.6	1.86±0.77	undefined	starburst	phot- <i>z</i>
GND13Jay	12:36:41.37	+62:11:29.5	1.03±0.01	disk	active	<i>HST</i> +WFC3
GND13Sto	02:37:16.59	+62:16:43.4	1.80±0.02	undefined	active	phot- <i>z</i>
GSD10Pri	03:32:37.99	-27:46:38.7	1.550±0.0001	irregular	starburst	VLT+X-Shooter
GSD11Was	03:32:20.86	-27:49:41.5	1.042±0.23	disk	starburst	<i>HST</i> +WFC3
UDS10Wil	02:17:46.33	-05:15:23.9	1.914±0.001	spheroid	starburst	VLT+X-Shooter

^a Photometric redshifts are marked as “phot-*z*” and spectroscopic redshifts are labeled with the observatory and instrument employed.

^b No plausible host galaxy was identified for SN COS12Car. The coordinates given are for the SN itself.

Table 4
SALT2 Light-Curve Fit Parameters

SN ID	m_B	x_1	c	$\Delta\mu_{\text{bias-corr}}$	μ (mag)	Notes
CLA10Cal	-	-	-	-	-	poor light-curve fit
CLF11Ves	25.38 (0.091)	-1.24 (0.60)	-0.288 (0.101)	+0.27	25.73 (0.34)	
CLH11Tra	25.30 (0.095)	-3.35 (2.10)	-0.272 (0.090)	-	-	fails x_1 cut ($x_1 < -3$, $\sigma_{x_1} > 1$)
CLP12Get	25.73 (0.088)	+1.01 (0.95)	-0.139 (0.098)	+0.18	26.06 (0.28)	
COS12Car	26.14 (0.122)	+2.35 (0.83)	+0.152 (0.083)	+0.07	25.91 (0.21)	
EGS11Oba	-	-	-	-	-	poor light-curve fit
EGS13Rut	25.92 (0.071)	+0.98 (1.08)	+0.055 (0.046)	-0.07	25.93 (0.20)	
GND12Col	26.81 (0.056)	+0.02 (0.91)	+0.128 (0.133)	-0.50	26.88 (0.25)	
GND13Cam	25.91 (0.061)	-1.35 (0.48)	-0.083 (0.043)	-	-	Hubble diagram outlier ($> 4\sigma$)
GND13Gar	25.42 (0.259)	+0.02 (0.99)	+0.310 (0.179)	-	-	fails color cut ($c > 0.3$)
GND13Jay	24.56 (0.672)	-2.04 (0.92)	-0.373 (0.447)	-	-	fails color cut ($c < -0.3$)
GND13Sto	26.15 (0.074)	-0.48 (0.70)	+0.000 (0.071)	-0.17	26.20 (0.19)	
GSD10Pri	25.76 (0.089)	-0.51 (0.41)	-0.186 (0.078)	+0.16	26.01 (0.19)	
GSD11Was	25.32 (0.057)	+1.04 (0.67)	-0.089 (0.039)	+0.09	25.60 (0.15)	
UDS10Wil	26.28 (0.172)	-1.64 (0.76)	+0.082 (0.152)	-0.43	26.15 (0.26)	

et al. 2009), the Pan-STARRS1 Medium-Deep Survey (PS1, Rest et al. 2014), and the Canada-France-Hawaii Telescope Supernova Legacy Survey (SNLS, Conley et al. 2011). The compilation includes all SNe from the Rest et al. (2014) sample and from the samples included in the joint light-curve analysis (JLA; Betoule et al. 2014), all uniformly calibrated as presented in the Supercal analysis (Scolnic et al. 2015). The Pantheon compilation also includes 12 equivalently high-confidence SNe Ia at $1 < z < 1.4$ from past *HST* SN surveys (see Table 5), 9 from Riess et al. (2004) and Riess et al. (2007) and 3 from Suzuki et al. (2012), that meet the criteria given in Scolnic et al. (2017).

3. HIGH-REDSHIFT MEASUREMENTS OF THE HUBBLE PARAMETER

At $z \gtrsim 1$, dark energy is a small contribution to the energy budget ($\rho_\Lambda/\rho \approx 0.2$ at $z = 1$ and ≈ 0.1 at $z = 1.5$) and therefore has a small effect on dynamics. With abundant and better-measured SNe at lower redshifts, constraints on typical one-or-two-parameter dark energy models are only weakly improved by observations of SNe at $z > 1$ (see also Andersen & Hjorth

2017, regarding $z > 2$). This is especially true for combined constraints when precise distances from cosmic microwave background (CMB) and baryon acoustic oscillations (BAO) measurements are included.

Nevertheless, the new SNe at $z > 1.5$ presented here allow us to constrain the (dimensionless) Hubble parameter $E(z) \equiv H(z)/H_0$ at greater redshifts than previously possible. The quantity $H(z)$ is particularly useful because it is both a direct probe of cosmology and still closely tied to the data. As a dynamical quantity, $H(z)$ contains information about the expansion history without reference to any physical cosmological model. Also, at least for current SN Ia data, the inferred $H(z)$ measurements are fairly local; that is, they are predominantly influenced by SNe at nearby redshifts. The quantity $E(z)$, which contains similarly useful information but can be measured using SN Ia data alone, makes the results independent of uncertainties associated with the determination of the absolute distance scale of SNe Ia (Riess et al. 2016).

As a direct probe of the expansion rate ($H \equiv \dot{a}/a$), measurements of $E(z)$ are particularly dense with cos-

Table 5
SNe Ia at $z > 1$ from Other Surveys

SN ID	Nickname	Survey ^a	Confidence ^b	Redshift	Reference
1997ff	1997ff	HDFN	Gold	1.755	Riess et al. 2001
2002fw	Aphrodite	Higher-z GOODS	Gold	1.30	Riess et al. 2004
2002fx	Athena	Higher-z GOODS	Silver	1.40	Riess et al. 2004
2002hp	Thoth	Higher-z GOODS	Gold	1.305	Riess et al. 2004
2002ki	Nanna	Higher-z GOODS	Gold	1.141	Riess et al. 2004
2003aj	Inanna	Higher-z GOODS	Silver	1.307	Riess et al. 2004
2003ak	Gilgamesh	Higher-z GOODS	Silver	1.551	Riess et al. 2004
2003az	Torngasak	Higher-z GOODS	Silver	1.265	Riess et al. 2004
2003dy	Borg	Higher-z GOODS	Gold	1.34	Riess et al. 2004
HST04Eag	Eagle	Higher-z PANS	Gold	1.019	Riess et al. 2007
HST04Gre	Greenburg	Higher-z PANS	Gold	1.14	Riess et al. 2007
HST04Mcg	Mcguire	Higher-z PANS	Gold	1.357	Riess et al. 2007
HST04Sas	Sasquatch	Higher-z PANS	Gold	1.39	Riess et al. 2007
HST05Fer	Ferguson	Higher-z PANS	Gold	1.02	Riess et al. 2007
HST05Gab	Gabi	Higher-z PANS	Gold	1.12	Riess et al. 2007
HST05Koe	Koekemoer	Higher-z PANS	Gold	1.23	Riess et al. 2007
HST05Lan	Lancaster	Higher-z PANS	Gold	1.235	Riess et al. 2007
HST05Str	Strolger	Higher-z PANS	Gold	1.027	Riess et al. 2007
SCP0401	SCP0401	SCP GOODS	Gold	1.713	Rubin et al. 2013
SCP05D0	Frida	SCP CSS	Gold	1.014	Suzuki et al. 2012
SCP05D6	Maggie	SCP CSS	Gold	1.315	Suzuki et al. 2012
SCP06A4	Aki	SCP CSS	Silver	1.192	Suzuki et al. 2012
SCP06C0	Noa	SCP CSS	Gold	1.092	Suzuki et al. 2012
SCP06F12	Caleb	SCP CSS	Silver	1.110	Suzuki et al. 2012
SCP06G4	Shaya	SCP CSS	Gold	1.35	Suzuki et al. 2012
SCP06H5	Emma	SCP CSS	Gold	1.231	Suzuki et al. 2012
SCP06K0	Tomo	SCP CSS	Gold	1.415	Suzuki et al. 2012
SCP06K18	Alexander	SCP CSS	Silver	1.411	Suzuki et al. 2012
SCP06N33	Naima	SCP CSS	Silver	1.188	Suzuki et al. 2012
SCP06R12	Jennie	SCP CSS	Gold	1.212	Suzuki et al. 2012
SCP06U4	Julia	SCP CSS	Gold	1.05	Suzuki et al. 2012

^a *HDFN*: SN 1997ff was discovered in observations of the Hubble Deep Field North (HDFN; Gilliland et al. 1999; Dickinson et al. 2001).

Higher-z GOODS/PANS: Discoveries by the Hubble Higher-z SN Search team, from the SN component of the Great Observatories Origins Deep Survey (GOODS, HST-GO-9728, HST-GO-9352, HST-GO-9583; Giavalisco et al. 2004; Strolger et al. 2004) and the successor program Probing Acceleration Now with Supernova (PANS, HST-GO-10339; Riess et al. 2007).

SCP-GOODS/CSS: Discoveries by the Supernova Cosmology Project (SCP) on the GOODS fields (HST-GO-9727) or in the Cluster Supernova Search (CSS, HST-GO-9425; Dawson et al. 2009).

^b Confidence in the Type Ia classification, as reported by Riess et al. (2007) or Suzuki et al. (2012), where the latter have been translated from “secure/probable/plausible” to “gold/silver/bronze.”

mological information. They provide, for instance, a straightforward way to test or falsify a given cosmological model (Mortonson et al. 2009, 2010; Shafieloo & Clarkson 2010). Given current constraints on its parameters, the flat Λ CDM model already makes very precise predictions for such basic observables. Constraints on the matter density Ω_m from combined probes (e.g., Ade et al. 2016) imply that $E(z)$, defined to be exactly one at $z = 0$, is predicted to a precision ranging from $\sim 0.1\%$ at $z = 0.1$ to $\sim 1\%$ at $z = 2$. Therefore, any new, independent measurement of $E(z)$, particularly in a new redshift range, is a direct and nontrivial test of the standard cosmological model. Given the present $> 3\sigma$ tension between $H(z)$ calibrated at $z \approx 0$ (Riess et al. 2016) and at $z \approx 1100$ by the CMB (Ade et al. 2016), it is especially worthwhile to see if the expansion rate fails to match the standard Λ CDM model prediction anywhere along this redshift range.

Furthermore, as we will illustrate, accurate estimates of $E(z)$ from SN Ia data are a convenient and efficient form of data compression, allowing one to obtain SN Ia constraints on dark energy and other cosmological parameters quickly and robustly using a very small and

easily provided set of measurements. Such data compression techniques will be especially useful as SN Ia samples grow significantly in size in the coming decade. Some recent SN Ia analyses (e.g., Betoule et al. 2014) have included compressed versions of the SN data in the form of binned distance moduli, and it is worth investigating the extent to which $E(z)$ measurements can serve a similar purpose.

Finally, quantifying SN Ia constraints on $E(z)$ facilitates a more direct comparison with other cosmological probes of geometry, such as anisotropic fits of the BAO feature, which effectively constrain a dimensionless measure of the expansion rate, the product of the Hubble parameter and the sound horizon, where the latter is inferred precisely from CMB observations.

Our aim here is to employ a new, well-calibrated compilation of SNe Ia, featuring the final addition of 9 new SNe Ia at $z > 1$ from the CANDELS and CLASH programs, to obtain unbiased estimates of the Hubble parameter $E(z)$ up to $z \approx 1.5$.

In what follows, we will briefly review some proposed methodologies for inferring $E(z)$ from SN Ia data (Sec-

tion 3.1) and then discuss our approach and how it overcomes some important limitations (Section 3.2). In Section 3.3, we present constraints on $E(z)$ for the Pantheon SN compilation supplemented by the MCT SNe (i.e., Pantheon + MCT²⁵). We illustrate how the handful of high-redshift SNe from CANDELS and CLASH significantly improves the determination of $E(z)$ at $z \approx 1.5$. We also illustrate the effectiveness of the $E(z)$ measurements in subsequent inference of cosmological parameters, and, in Section 3.4, the ability of the high-redshift SNe Ia to distinguish cosmology from SN Ia evolution. Finally, employing a realistic simulation of a potential *WFIRST* SN survey observing strategy, we compare our current results with optimistic future constraints on $E(z)$ (Section 3.5).

3.1. SN Ia Measurements of $E(z)$

SNe Ia measure distances most directly; roughly speaking, each SN provides an independent measurement of the luminosity distance to its redshift. For a flat universe, we have

$$d_L(z) = \frac{c}{H_0} (1+z) \int_0^z \frac{dz'}{E(z')} ; \quad (1)$$

therefore the (inverse) Hubble parameter, the derivative of the comoving distance, must be inferred indirectly when starting from raw SN Ia data.

A variety of interrelated methods have been used for this purpose. Some analyses have focused on model-independent reconstruction of an analytical $E(z)$ function or of other dynamical quantities like the deceleration parameter $q(z)$ (Shafieloo et al. 2006; Sahni & Starobinsky 2006; Shafieloo 2007; Ishida & de Souza 2011). Such reconstructions are useful for understanding where the data are most constraining, and they can indicate whether the functional form for $H(z)$ naturally preferred by the data is consistent with that of a physical model like Λ CDM. On the other hand, it is not possible, or at least not straightforward, to subsequently incorporate the reconstructions in a likelihood function, or otherwise in a statistical analysis, in order to constrain cosmological parameters.

Other methods focus on obtaining direct measurements of $E(z)$ at several redshifts by smoothing and/or weighting the individual SNe and differentiating the distance-redshift relation (Tegmark 2002; Daly & Djorgovski 2003, 2004). One proposed method (Wang & Tegmark 2005), which has been employed in some subsequent analyses (Riess et al. 2007; Mortsell & Clarkson 2009; Avgoustidis et al. 2009), seeks direct, independent estimates of $E(z)$ in redshift bins by first converting SN distance moduli into their corresponding comoving distances r_i , then transforming these r_i into noisy, but locally unbiased, estimates of $E(z)^{-1}$ between neighboring SNe. A specific weighted average then yields a minimum-variance estimate of $E(z)^{-1}$ over a wider redshift bin. We have verified numerically that this procedure is actually *equivalent* to the weighted least-squares fit of a line to the r_i vs. z_i data over the same wide redshift bin, where the slope corresponds to $E(z)^{-1}$. Both the least-squares

estimator and that of Wang & Tegmark (2005) have been shown to be unbiased and have minimum variance, assuming SN redshifts are exact and $E(z)$ is constant over the redshift bin, so it is not surprising that these estimators coincide.

While such an approach is attractive in that it directly transforms the SN distances into independent measurements of $E(z)$ at different redshifts, it has notable problems that make it unsuitable in practice. The first step requires converting SN distance moduli into comoving distances, and one must therefore assume a value for the intercept of the Hubble diagram, which is unknown *a priori*. As this quantity is partially degenerate with $E(z)$, particularly the lowest-redshift measurement, fixing the intercept to some best-fit value would artificially remove a degree of freedom from the fit, resulting in underestimated uncertainties. One could instead interpret the estimates as estimates of $AE(z)^{-1}$, where A is an arbitrary constant. In this case, though, properly extracting cosmological information from the $E(z)$ measurements would require fully marginalizing over A in a fit to multiple measurements of $AE(z)^{-1}$.

Furthermore, an $E(z)$ estimate using this method reflects some average of $E(z)$ over the redshift bin, not necessarily the value at the bin's center. Unless $E(z)$ is constant over the redshift bin, this will lead to a bias, and since only a handful of $E(z)$ values can be constrained robustly with current data, one might expect the bias to be significant. Indeed, by simulating instances of our SN data (see Section 3.2), we have verified that biases in such $E(z)$ estimates are typically a large fraction (~ 0.5) of their uncertainty, making the measurements unsuitable for later cosmological inference.

3.2. Parametrized $E(z)$ and Interpolation

We now describe a somewhat different approach for determining $E(z)$ from SN Ia data. We explain how it avoids the problems discussed in Section 3.1 and provides more meaningful and robust $E(z)$ measurements. We will assume that the true, underlying $E(z)$ function is a continuous, smooth function of redshift, which is certainly the case for most physical and empirical models studied in the literature.

In our approach, we parametrize $E(z)$ by its value at several specific redshifts and employ a basic interpolation scheme to define the complete $E(z)$ function, which can then be numerically integrated to compute the luminosity distance and compare to the data. This allows us to constrain the $E(z)$ parameters using the full SN dataset in its raw form, as one would in a standard dark energy analysis. This way, any nuisance parameters associated with the SN data, notably the distance scale or Hubble diagram intercept, can be properly marginalized over in the fit.

While the total number of $E(z)$ values to constrain is somewhat arbitrary, there are several considerations. Choosing too many $E(z)$ parameters results in weaker constraints and posterior distributions that are less likely to be Gaussian. Choosing too few $E(z)$ values increases the chance that the estimates will be biased, as the interpolating function will deviate from the functional form of the underlying cosmology. The specific redshifts, while also somewhat arbitrary, should reflect the redshift range and distribution of the SNe. Since the $E(z)$ measure-

²⁵ Note that the Pantheon compilation as defined in Scolnic et al. (2017) includes the MCT SNe presented here.

ments, especially those at neighboring redshifts, will naturally be somewhat correlated, choosing too small a separation in redshift between a given pair will lead to undesirably large pairwise correlations in the estimates.

Overall, we find that employing a shape-preserving piecewise-cubic Hermite interpolating polynomial (implemented as `pchip` in MATLAB; see Kahaner et al. 1988) to interpolate (and extrapolate) the $E(z)$ function works particularly well, though other interpolation schemes (various splines, simple linear interpolation) are also generally suitable. For any specified $E(z)$ (any fiducial cosmology), it is straightforward to determine whether the $E(z)$ estimates resulting from the interpolation and fitting procedure are unbiased. To check this, we repeatedly simulate instances of our SN Ia data; that is, we keep the same SN redshifts and covariance matrix as the real SN data, but repeatedly sample the distance moduli from a multivariate Gaussian centered on the fiducial cosmology. Of course, unbiased constraints for the fiducial cosmology do not guarantee unbiased results for other cosmologies. In principle, one could perform this check for each specific model of interest; however, there is reason to worry only when a model predicts $E(z)$ to vary rapidly or have features too narrow to be captured by the widely spaced $E(z)$ parameters. For the highest-redshift SNe Ia, a modest amount ($\sim 25\%$) of the integral of $E(z)^{-1}$ must be evaluated via extrapolation beyond the last redshift anchor of the $E(z)$ function. However, our simulations indicate that this does not bias this highest-redshift measurement of $E(z)$. Indeed, we have verified that all of the $E(z)$ measurements are biased by $\lesssim 10\%$ of their individual statistical uncertainties.

In essence, our procedure trades the ability to make direct, independent measurements of $E(z)$ at redshifts that are somewhat uncertain (and not randomly so) for the ability to obtain precise, unbiased $E(z)$ estimates at specific redshifts. Only this latter type of estimate allows for accurate subsequent cosmological inference with the $E(z)$.

3.3. SN Ia Constraints on $E(z)$

We now constrain $E(z)$ for the Pantheon compilation of 1039 SNe Ia, which we will supplement with the high-redshift CANDELS and CLASH SNe. The Pantheon compilation (Scolnic et al. 2017, in prep.) includes data from multiple surveys (CfA(1–4), CSP, SDSS, SNLS, Pan-STARRS1, *HST*) calibrated for a joint cosmological analysis. Below we summarize the key aspects of the Pantheon analysis, and we refer the reader to Scolnic et al. (2017) for additional details and a complete discussion.

The Pantheon analysis presents the full set of spectroscopically confirmed SNe Ia from the Pan-STARRS1 (PS1) Medium Deep Survey, building on the earlier analysis of the first 1.5 yr of PS1 (Rest et al. 2014; Scolnic et al. 2014). It relies on the Supercal cross-calibration procedure presented by Scolnic et al. (2015), which uses the relative consistency of the Pan-STARRS1 photometry over 3π steradians of the sky to tie together the photometric systems of the individual surveys. The Pantheon analysis also incorporates the BBC methodology of Kessler & Scolnic (2017) (see also Scolnic & Kessler 2016), which corrects for distance biases dependent on

the light-curve properties of the SNe and the surveys from which they are selected.

The Pantheon analysis employs the SALT2 light-curve fitter (Guy et al. 2007; Betoule et al. 2014), which determines an overall normalization of the log-flux (m_B), a shape parameter (x_1), and a color (c) for each SN light curve, along with associated uncertainties. We standardize the SNe by modeling an individual SN Ia distance modulus as

$$\mu = m_B - M + \alpha x_1 - \beta c + \Delta_M + \Delta_B. \quad (2)$$

The Δ_M term is an additional correction for the empirical host-mass step, where SNe in high-stellar-mass host galaxies ($\log_{10}(M_*/M_\odot) \gtrsim 10$) are ~ 0.05 mag brighter on average, after light-curve standardization. The Δ_B term represents the distance bias correction. Note that M , α , β , and the amplitude of the mass step (included in the Δ_M term) are all nuisance parameters that must be determined by a fit to the data. In our analysis, only M (effectively, the Hubble diagram offset) is fit along with the cosmological parameters $E(z)$. The other parameters are well determined independently of cosmology in the Pantheon analysis. The inferred values are $\alpha \approx 0.15$ – 0.16 and $\beta \approx 3.0$ – 3.7 , where the results vary depending on the intrinsic scatter model²⁶. Finally, note that the distance modulus as predicted by the cosmological model is given by

$$\mu(z) = 5 \log_{10} \left[\frac{d_L(z, \mathbf{p})}{1 \text{ Mpc}} \right] + 25, \quad (3)$$

where d_L is the luminosity distance, which is a function of redshift and also depends on the set of cosmological parameters \mathbf{p} .

The statistical uncertainties of SN distance moduli are modeled, in the standard way, as a combination of observational measurement uncertainty, intrinsic scatter, and additional scatter due to gravitational lensing, peculiar velocities, and redshift measurement uncertainty²⁷. The inferred value for the intrinsic scatter is $\sigma_{\text{int}} \approx 0.1$, although, like α and β , the value depends on the intrinsic scatter model. After bulk-flow corrections are applied to the low-redshift SNe, we add a peculiar-velocity scatter of $\sigma_v = 250 \text{ km s}^{-1}$. We assume a value $\sigma_{\text{lens}} = 0.055z$ for the lensing scatter (Jönsson et al. 2010). Note that the distribution of the shift in observed magnitude due to lensing is non-Gaussian (e.g., Jönsson et al. 2006), with a tail of strongly magnified SNe; however, by examination of foreground structures we have verified that none of our CANDELS or CLASH SNe are likely to fall in this tail, making the lensing scatter contribution to the distance uncertainty a good approximation. Note that there is also statistical uncertainty in the host-mass correction and the distance bias correction.

²⁶ In the Pantheon analysis, two alternative models for the intrinsic scatter are separately used to derive distance bias corrections, which are then averaged, with half of the difference included in the systematic uncertainty budget.

²⁷ Separate from standard propagation of redshift uncertainty, the derived distance moduli themselves depend on the observed redshift. We have verified that, for SN GND12Col, which has a large redshift uncertainty with asymmetric errors, repeating the analysis with both its redshift and distance shifted by 1σ does not significantly affect the results.

Table 6
Pantheon + MCT SN Ia Measurements of $E(z)$

z	$E(z)^{-1}$ ^a	Correlation Matrix							$E(z)$	Distance Residual $\Delta\mu/(0.01 \text{ mag})$ ^b
0.07	1.003 ± 0.023	1.00							0.997 ± 0.023	-0.13 ± 0.99
0.2	0.901 ± 0.017	0.39	1.00						1.111 ± 0.020	-0.23 ± 1.26
0.35	0.887 ± 0.029	0.53	-0.14	1.00					1.128 ± 0.037	$+0.23 \pm 1.32$
0.55	0.732 ± 0.033	0.37	0.37	-0.16	1.00				1.364 ± 0.063	$+0.11 \pm 1.97$
0.9	0.656 ± 0.052	0.01	-0.08	0.17	-0.39	1.00			1.52 ± 0.12	$+1.15 \pm 2.85$
1.5	0.342 ± 0.079	-0.02	-0.08	-0.07	0.15	-0.19	1.00		$2.67^{+0.83}_{-0.52}$	-3.42 ± 6.78

^a Mean and standard deviation of the marginalized likelihood, approximately Gaussian in all cases.

^b Effective distance moduli relative to those of a fiducial Λ CDM cosmology ($\Omega_m = 0.3$), as determined by an interpolated fit to the residuals using the same redshift control points as the $E(z)$ analysis.

The Pantheon analysis also includes a rigorous analysis of systematic errors, adding terms to the covariance matrix of SN distances to account for uncertainties in photometric calibration (including terms for individual survey calibration, the Supercal cross-calibration procedure, and the SALT2 model itself), the intrinsic scatter model, survey selection functions, Milky Way dust extinction, β evolution, the host mass step and its evolution, and peculiar velocity coherent flow corrections.

Standard data-quality cuts were applied to remove SNe that are not expected to follow the empirical standardization relations. Specifically, we keep only SNe with $|x_1| < 3$, $\sigma_{x_1} < 1$, $|c| < 0.3$, a light-curve fit with $\chi^2/N_{\text{dof}} < 3$, and an uncertainty in the time of peak brightness of less than 2 days. Similar cuts have been used in most recent SN Ia cosmological analyses (e.g., Betoule et al. 2014; Rest et al. 2014; Riess et al. 2016). These cuts eliminate 3 of the silver and gold MCT SNe (CLH11Tra, GND13Gar, GND13Jay; see Table 4). Finally, a 4σ outlier rejection from the best-fit Hubble diagram is applied and removes GND13Cam, leaving 9 *HST* MCT SN Ia in the joint analysis²⁸. Note that here we do include EGS13Rut, which is on the edge of the σ_{x_1} cut but has typical light-curve fit parameters. Although the final MCT addition of 9 SNe represents $< 1\%$ of the combined sample, the unusually-high redshifts (7 with $z > 1.5$) provide unique leverage on $E(z)$ at $z = 1.5$.

Following the methodology and discussion in Section 3.2, we parametrize $E(z)^{-1}$ by its value at six redshifts (chosen to best summarize the sample) and therefore have six free parameters to constrain. It is important to remember that the Hubble diagram offset is a free parameter as well, though we analytically marginalize over this offset, with a flat prior, in the likelihood. We assume a flat universe ($\Omega_k = 0$) throughout, so the $E(z)$ measurements are cosmological-model-dependent in this sense. To obtain the constraints, we sample the likelihood using a custom Markov chain Monte Carlo (MCMC) code employing the basic Metropolis-Hastings algorithm. We impose flat, hard-bound priors on the $E(z)^{-1}$ parameters wide enough that extending the bounds does not affect the resulting constraints. The final MCMC chains were inspected to verify convergence.

The resulting marginalized posterior likelihoods for

²⁸ In the Pantheon analysis, additional cuts were applied to remove SNe without an observation at least 5 days after peak brightness and with light-curve parameters that do not fall in the simulated distribution from the BBC method (see Scolnic et al. 2017). These cuts do not remove any of the remaining MCT SNe.

$E(z)^{-1}$ are Gaussian to a good approximation, and the constraints are given in Table 6. In Figure 1, we convert the measurements of $E(z)^{-1}$ into $E(z)$ measurements by reprocessing the MCMC chains and then compare the results with and without the MCT SNe. It is not surprising that the MCT SNe substantially improve the measurement of $E(z)$ at $z = 1.5$. They permit a $\sim 20\%$ measurement of $E(z = 1.5)$, roughly a factor of three improvement over the result without the MCT SNe. While the CANDELS and CLASH SNe mostly affect the measurement at $z = 1.5$, they also improve and shift some lower-redshift measurements, which are somewhat correlated ($\approx 8\%$ and 4% improvements at $z = 0.9$ and 0.55 , respectively). By eye, the set of $E(z)$ measurements may appear somewhat discrepant with the fiducial Λ CDM model, but the overall χ^2 , which includes the moderate correlations, is 5.6 for the 6 degrees of freedom.

In Figure 2, we scale $E(z)$ by $(1+z)^{-1}$ to illustrate the constraints on the time derivative of the scale factor $\dot{a}(z)$, relative to its present value, for the same data shown in Figure 1. In this space, it is clear that the low-redshift and high-redshift $E(z)$ measurements together provide evidence for both recent acceleration and earlier deceleration epochs, as predicted by standard cosmological models. In addition to the fiducial Λ CDM model, we show dynamical models with fixed deceleration parameter q_0 . The $\dot{a}(z)$ values track the $q_0 = -0.5$ model at $z \lesssim 0.5$ (where the low- z behavior matches that of a Λ CDM model with $\Omega_m \approx 0.3$) but show deceleration with respect to that curve at higher redshifts. The coasting cosmology ($q_0 = 0$), pure acceleration cosmology ($q_0 = -0.5$), and pure deceleration cosmology ($q_0 = 0.5$, equivalent to a flat CDM model with $\Omega_m = 1$) are strongly disfavored with $\Delta\chi^2 = 79.8$, $\Delta\chi^2 = 36.5$, and $\Delta\chi^2 = 360.2$, respectively, for 6 degrees of freedom. The measurement at $z = 1.5$ alone, while consistent with the other models, disfavors $q_0 = -0.5$ with $\Delta\chi^2 = 13.5$.

As an illustration of the power of the $E(z)$ measurements in constraining (spatially flat) cosmologies, we compare constraints on common dark energy parameterizations in Figure 3. Remarkably, the constraints are nearly identical whether the parameters are constrained with the SN Ia data directly or with the $E(z)$ measurements in Table 6. It may not be too surprising that $E(z)$ captures the constraining power of the SNe for simple one-or-two-parameter models. One would not expect the same for fits with many degrees of freedom (e.g., more complicated dark energy models); in practice, however, current and near-future SN Ia data can only meaningfully

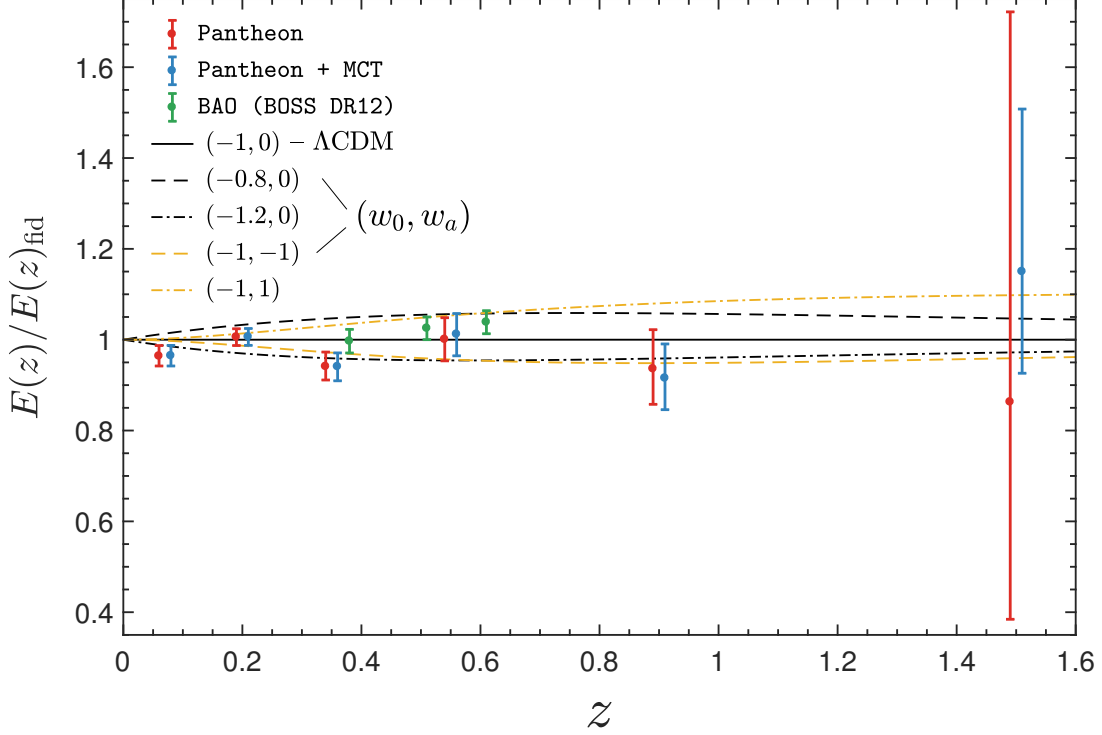


Figure 1. Constraints on $E(z) \equiv H(z)/H_0$, relative to $E(z)$ for a fiducial Λ CDM model ($\Omega_m = 0.3$). We compare the constraints with (blue points) and without (red points) the high-redshift CANDELS and CLASH (MCT) SNe Ia. Note that these $E(z)$ measurements are correlated and have non-Gaussian distributions (the error bars enclose 68.3% of the likelihood). For comparison, we also show the three (correlated) measurements of $E(z)$ from combined BOSS DR12 BAO data (Alam et al. 2016) after calibration with *Planck* Λ CDM constraints on $H_0 r_d$ (green points).

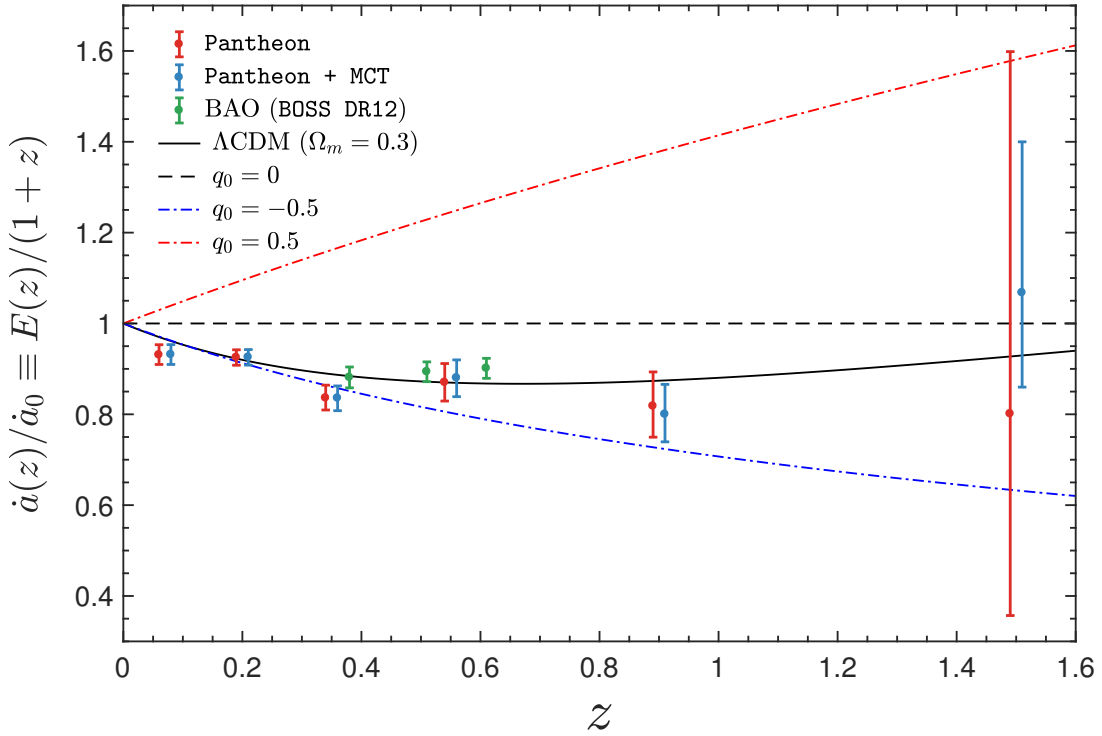


Figure 2. For the same data as in Figure 1, we show constraints on the time derivative of the scale factor $\dot{a}(z)$ relative to its present value, obtained by scaling the $E(z)$ values by $(1+z)^{-1}$. We compare the fiducial Λ CDM model to alternative models with a constant deceleration parameter $q_0 = 0$ (coasting cosmology), $q_0 = -0.5$ (pure acceleration), and $q_0 = 0.5$ (pure deceleration), all assuming a flat universe.

constrain 2–3 expansion parameters anyway. For models that assume a flat universe and predict fairly smooth, featureless $H(z)$, the $E(z)$ constraints will be an efficient summary of the present SN Ia data.

3.4. High-Redshift SNe Ia and Evolution

The use of SNe Ia as standardizable candles across redshift relies on the understanding that their uncommonly homogeneous luminosities and colors follow from their nature as carbon-oxygen white dwarfs close to the Chandrasekhar mass. While uncertainty persists regarding *how* these degenerate stars approach that mass limit, either by accretion from a nondegenerate companion or through the tidal disruption followed by accretion of a degenerate companion, there has long been agreement about this model based on the well-understood physics of degenerate stars (Hoyle & Fowler 1960; Arnett 1969; Colgate & McKee 1969). The thermonuclear detonation of a Chandrasekhar-mass carbon-oxygen white dwarf yields a mass of radioactive nickel whose energy output matches that of a SN Ia (Arnett et al. 1985) and whose modeled nucleosynthesis matches its spectral elements (Nomoto et al. 1984). More recently, pre-discovery observations of SN 2011fe, a prototypical SN Ia in M101, demonstrated that the progenitor did not exceed a radius of 2% solar, fully consistent with the expected white dwarf (Nugent et al. 2011; Li et al. 2011; Bloom et al. 2012). Yet the difficulty and low likelihood of ever directly observing a white dwarf system before it becomes a SN Ia leaves enough uncertainty and model freedom to support the consideration of redshift evolution of the standardized SN Ia luminosity.

From SN Ia observations spanning a wide range of redshifts and sampling the epochs when cosmic expansion accelerates and decelerates, it is possible to distinguish such evolution from the uncertain properties of dark energy (Riess & Livio 2006). As an illustration of the power of SNe Ia at $z > 1$ to separate evolution from cosmology, we briefly reconsider the analysis of Tutusaus et al. (2017), which shows that power-law cosmology, where the scale factor evolves as $a(t) \propto t^n$ for some exponent n , is an equally good fit to SN Ia data (primarily at $z < 1$) as the Λ CDM model (with Ω_m free) when the standardized luminosity is also allowed to vary with redshift according to some simplistic, empirical models of SN Ia evolution. Although such models are not astrophysically motivated, they may be useful for exploring the separation of other SN distance-dependent effects (e.g., grey extinction) from cosmological parameters.

Here, as an illustration, we consider Model B ($\Delta M(z) = \epsilon z^\delta$) from Tutusaus et al. (2017) with fixed $\delta = 0.3$. We separately fit both Λ CDM and power-law cosmology to our combined (Pantheon + MCT) data; in each case, we fit for the Hubble diagram intercept, a cosmological parameter (Ω_m or n), and the amplitude ϵ of the assumed intrinsic luminosity evolution. We compare these fits in Figure 4. Fitting only the SNe at $z < 1$, a power law with $n = 1.1$ is a slightly *better* fit to the SN Ia data than Λ CDM. Indeed, when analyzing the JLA compilation, which features only ~ 5 SNe at $z > 1$, Tutusaus et al. (2017) claims a mild preference for the power law (note that their analysis also included BAO and $H(z)$ information).

In contrast, when we include our 24 SNe at $z > 1$,

a nearly coasting (marginally accelerating) power-law cosmology (best fit $n = 1.04$) together with simplistic SN Ia evolution is no longer as good a fit as the Λ CDM model, with a relative probability of $\exp(-\Delta\chi^2/2) \approx 20\%$. Without invoking evolution (that is, fixing $\epsilon \equiv 0$), the Λ CDM model is a much better fit than the power-law model, with the latter strongly disfavored with $\Delta\chi^2_{\Lambda\text{CDM}} = 8.3$, a relative probability of 1.6%, when including the new SNe at $z > 1.5$. Meanwhile, assuming Λ CDM and fitting for the evolution amplitude ϵ yields a value consistent with zero, $\epsilon = 0.08 \pm 0.15$, so there is no motivation for including it based on astrophysical *or* empirical considerations. A more comprehensive investigation of SN Ia evolution and cosmology is underway (Shafer et al. 2017, in prep.).

We note the addition of the MCT SNe to the Pantheon compilation also further reduces the already-low likelihood of the “empty universe” solution where $\Omega_m \approx 0$ and $\Omega_\Lambda \approx 0$ in an $O\Lambda$ CDM universe, a location Nielsen et al. (2016) claimed to be marginally consistent ($\sim 3\sigma$) with SN data alone using unconventional priors on SN distributions, to the boundary of the 6σ contour.

3.5. $E(z)$ with *WFIRST*

The *Wide-Field Infrared Survey Telescope* (*WFIRST*) was the top space-based recommendation of the 2010 U.S. astronomy and astrophysics decadal survey. The mission is still in formulation, but current plans specify a 2.4 m primary mirror and include a wide-field instrument for cosmology. The cosmology science objectives, as detailed in the most recent report from the Science Definition Team (SDT; Spergel et al. 2015), will be accomplished through a combination of SN Ia, galaxy, and weak-lensing surveys.

The *WFIRST* SN survey is anticipated to yield a large sample of thousands of SNe, many at $z > 1$ with precise distances. These SNe will vastly improve upon the high-redshift $E(z)$ measurements available today, allowing nontrivial and precision tests of the Λ CDM model independent of the BAO and weak-lensing constraints in a redshift range that is currently not well constrained.

Here we wish to forecast realistic constraints on $E(z)$ from *WFIRST*. Typical forecasts (e.g., for dark energy figures of merit) rely on Fisher matrix formalism, which is exact only for Gaussian posterior distributions and otherwise underestimates parameter uncertainties. For SN Ia forecasts, one typically assumes idealized, or roughly estimated, redshift distributions and makes simple assumptions about the measurement error. Here instead we employ a detailed simulation of one potential observing strategy for the *WFIRST* SN survey (Hounsell et al. 2017). We then constrain the $E(z)$ parameters using the methodology of Section 3.2 that was employed in Section 3.3 for our current Pantheon + MCT data.

For our illustration, we consider the *Imaging All-z* strategy described by Hounsell et al. (2017). This particular strategy relies on multi-band imaging for classification and assumes follow-up spectroscopy will provide host-galaxy redshifts. Hounsell et al. (2017) also assumes a large external sample of 800 SNe at $z < 0.1$. As the size of future systematic uncertainties is hard to predict, Hounsell et al. (2017) simulates a range of scenarios, and here we opt for all-around optimistic assumptions about future systematic errors (for what this entails, see Houn-

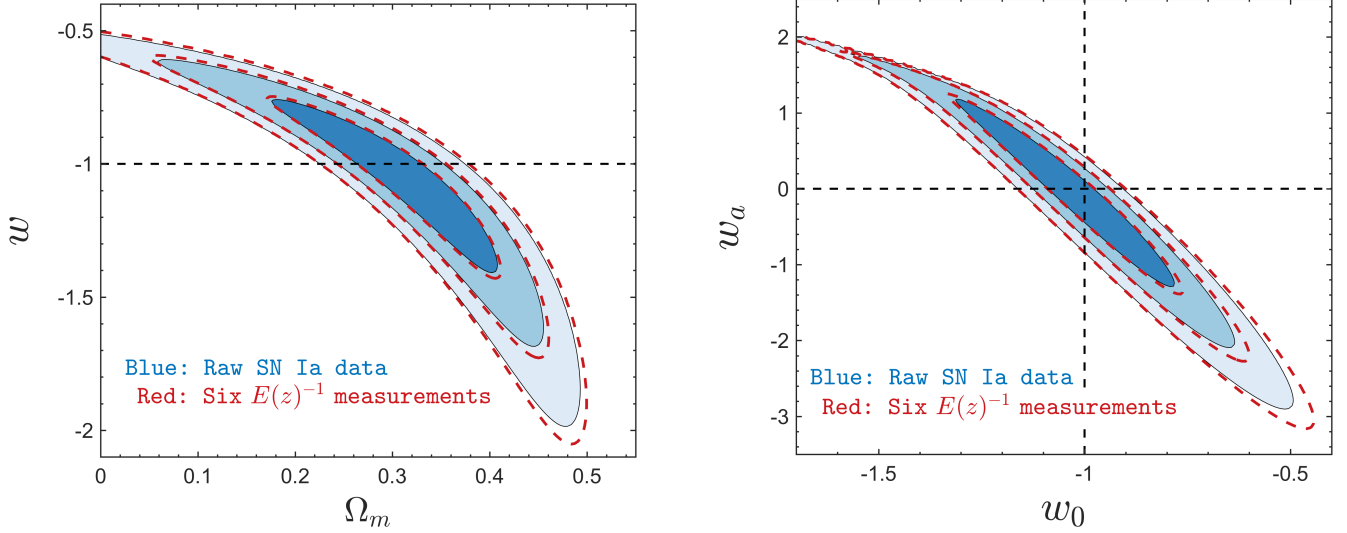


Figure 3. Constraints on Ω_m and a constant equation-of-state parameter w in a flat universe (left panel) and for the w_0 - w_a model (Chevallier & Polarski 2001; Linder 2003), marginalized over Ω_m and also assuming a flat universe (right panel). We compare the constraints when using the full SN Ia likelihood with individual distance moduli (filled blue contours) with the constraints from the six moderately correlated $E(z)$ measurements (open red contours). Contours contain 68.3%, 95.4%, and 99.7% of the likelihood, and for the w_0 - w_a constraints we have also included distance priors derived from *Planck* data (Ade et al. 2016).

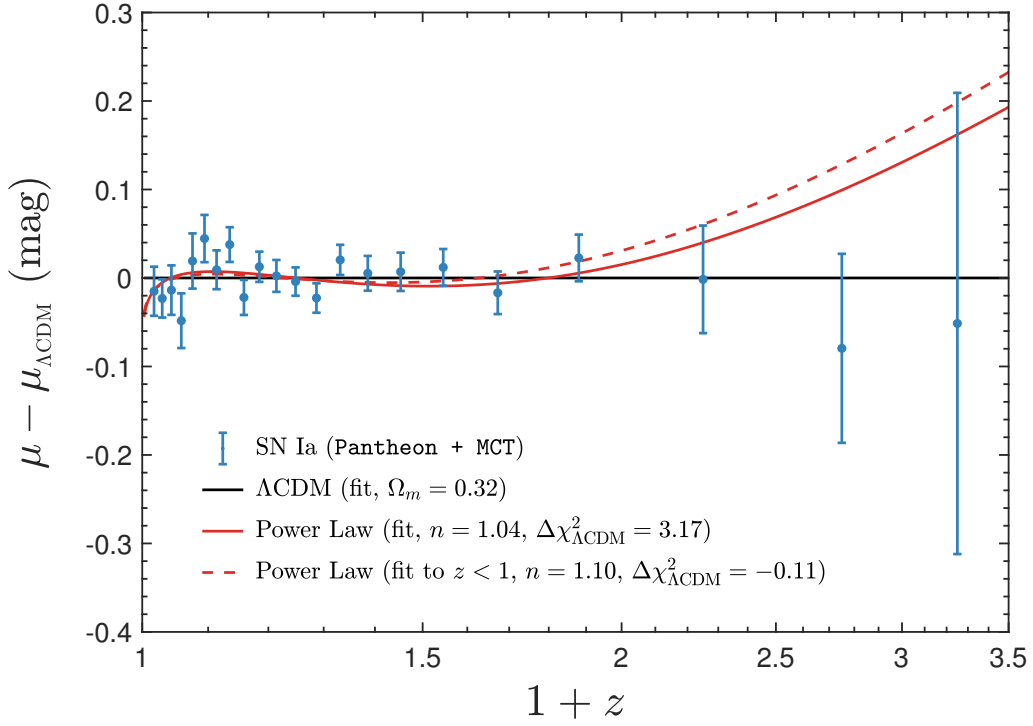


Figure 4. Comparison of ΛCDM and power-law cosmology ($a(t) \propto t^n$) fits to our SN Ia data, where in each case we allow the intrinsic luminosity to evolve as $\Delta M(z) = \epsilon z^\delta$, corresponding to Model B from Tutusaus et al. (2017), where we fix $\delta = 0.3$. The SN data are binned for clarity, and $\Delta\chi^2_{\Lambda\text{CDM}} \equiv \chi^2 - \chi^2_{\Lambda\text{CDM}}$.

Table 7
Simulated SN Ia
Measurements of $E(z)$ from
WFIRST

z	$E(z)$ Percent Error ^a
0.07	1.3
0.2	1.1
0.35	1.5
0.6	1.5
0.8	2.0
1.0	2.3
1.3	2.6
1.7	3.4
2.5	8.9

^a Note that these measurements are not fully independent; there are moderate pairwise correlations among some in the set. They assume a flat universe.

sell et al. 2017). In this scenario, the contribution of systematic errors is not negligible but is subdominant in the error budget.

In Figure 5, we compare our current Pantheon + MCT constraints on $E(z)$ with simulated constraints from the *WFIRST* Imaging All- z strategy. We find that we are able to constrain $E(z)$ robustly, albeit with moderate pairwise correlations, at 9 redshifts in the range $0.07 < z < 2.5$. In Table 7, we list the percent errors for $E(z)$ corresponding to our forecast. Note that these results are negligibly changed whether we quote percent errors on $E(z)$ or its inverse. We find that *WFIRST* allows 8 measurements of $E(z)$ at the 1–3% level, along with a robust but less precise measurement at $z \approx 2.5$. Notably, this is a constraint on the expansion rate at a redshift higher than any SN Ia has even been observed to date.

4. SUMMARY AND CONCLUSIONS

In this study, we analyzed the set of 15 high-redshift SNe Ia from the CANDELS and CLASH *HST* MCT programs, 9 of which ultimately pass classification confidence and quality cuts and 7 of which are at $z > 1.5$ where the relative expansion rate is poorly constrained. These are the first distance estimates for these SNe that are suitable for a joint cosmological analysis with a large compilation of lower-redshift SNe (the Pantheon compilation). We have introduced and employed a procedure to obtain unbiased constraints on the scale-free Hubble parameter $E(z) \equiv H(z)/H_0$ using only this extended Pantheon + MCT sample of SNe Ia (Table 6, Figures 1–2). The CANDELS and CLASH SNe at $z \gtrsim 1.5$ extend the Hubble diagram and allow us to achieve a robust measurement of the expansion rate at $z = 1.5$ that efficiently summarizes the cosmological leverage of these new SNe. Our measurement of $E(z = 1.5)^{-1} = 0.342 \pm 0.079$ (equivalently, $E(z = 1.5) = 2.67^{+0.83}_{-0.52}$) assumes a flat universe and smooth expansion history but is otherwise model-independent.

We also have demonstrated that the set of $E(z)$ measurements can serve as a form of SN Ia data compression, allowing us to summarize SN Ia constraints on spatially flat cosmological models that feature a smooth expansion history, which comprise the majority of the commonly studied dark energy models. The $E(z)$ are very econom-

ical, accurately reproducing parameter posteriors (even when non-Gaussian) using just 6 measured quantities in place of > 1000 (Figure 3). The computation time for this $E(z)$ likelihood, relative to that for the full SN Ia likelihood, is negligible.

Future large, high-quality samples of high-redshift SNe Ia, notably from *WFIRST*, will allow precision constraints on the dark energy equation-of-state parameter w , especially for dynamical dark energy featuring a time-varying value of w . Still, there are uses for such high-redshift SNe beyond direct dark energy constraints, inspiring us to perform two additional investigations.

First, using our combined Pantheon + MCT set of SNe Ia, we have briefly illustrated how the added leverage of our larger sample of SNe at $z > 1$, including 7 at $z > 1.5$, can help distinguish empirical SN Ia evolution and nonstandard cosmological models from the Λ CDM model (Figure 4). We have shown that, while a nearly coasting power-law model ($a(t) \propto t^n$ with $n \approx 1$) is as good a fit to the $z < 1$ data as Λ CDM (at least when certain forms of SN evolution are allowed), adding the $z > 1$ SNe disfavors the power law, indicating a relative probability of $\sim 20\%$, even when permitting the same SN evolution.

Second, we have used our $E(z)$ procedure in conjunction with a realistic simulation of a potential *WFIRST* SN Ia observing strategy to forecast optimistic *WFIRST* constraints on $E(z)$. We find that *WFIRST* will permit 8 measurements of $E(z)$ at the 1–3% level across a wide range of redshifts, along with a robust measurement at $z \approx 2.5$ (Figure 5, Table 7). Such measurements will constitute precise tests of our expectations from the Λ CDM model separately from BAO and other high-redshift distance probes.

Acknowledgments:

We thank Rebekah Hounsell for providing the *WFIRST* SN Ia simulations. It is our pleasure to thank program coordinators Patricia Royle and Beth Perriello, as well as the entire Space Telescope Science Institute (STScI) scheduling team, for their tireless efforts that made the CANDELS survey and the SN follow-up program possible.

This work was principally based on observations made with the NASA/ESA *Hubble Space Telescope*, which is operated by the Association of Universities for Research in Astronomy (AURA), Inc., under NASA contract NAS5-26555. These observations are associated with program IDs 12060, 12061, 12062, 12442, 12443, 12444, 12445, 12099, 12461, and 13063. The analysis presented here made extensive use of the Mikulski Archive for Space Telescopes (MAST). STScI is operated by AURA, Inc., under NASA contract NAS5-26555. Support for MAST for non-*HST* data is provided by the NASA Office of Space Science via grant NNX13AC07G and by other grants and contracts. Some of the data presented herein were obtained at the W.M. Keck Observatory, which is operated as a scientific partnership among the California Institute of Technology, the University of California, and NASA; the Observatory was made possible by the generous financial support of the W.M. Keck Foundation.

Financial support was broadly provided by NASA through grants HST-GO-12060 and HST-GO-12099 from

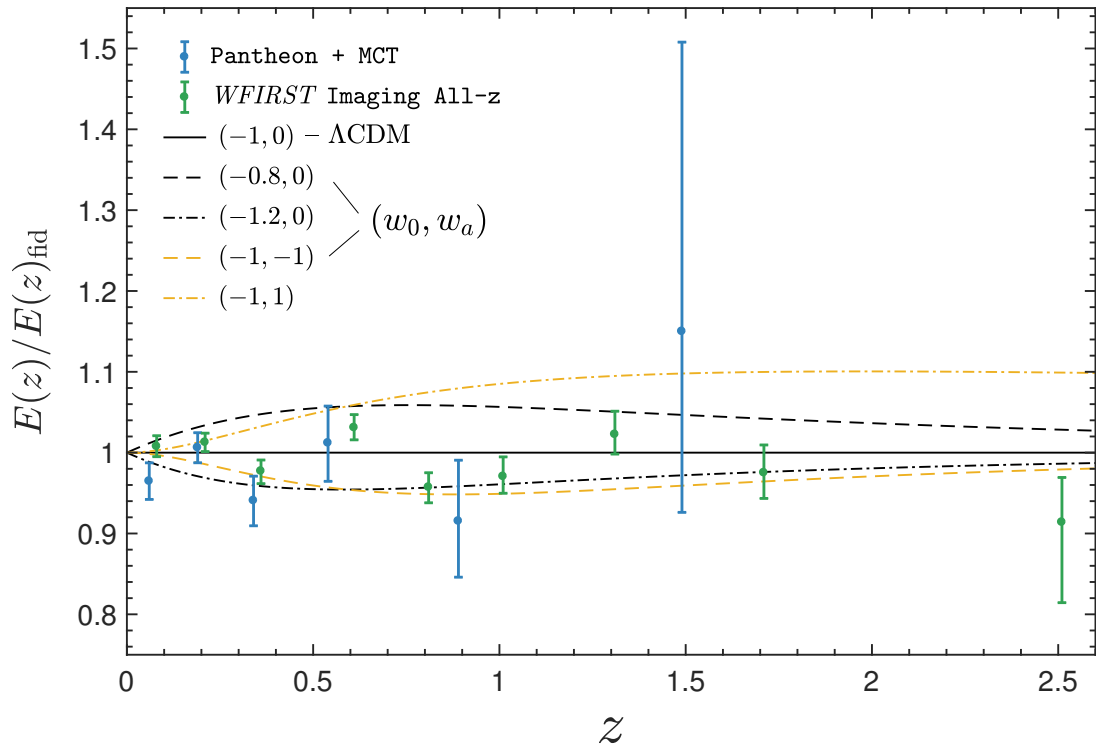


Figure 5. Simulated *WFIRST* constraints on $E(z) \equiv H(z)/H_0$, relative to $E(z)$ for a fiducial Λ CDM model ($\Omega_m = 0.3$). We compare the constraints from current data (blue points) with simulated constraints from the *WFIRST* Imaging All- z observing strategy (green points). We overlay the same dark energy models as in Figure 1.

STScI, and to S.A.R. through grant HST-HF-51312. A.V.F. is also grateful for generous financial assistance from the Christopher R. Redlich Fund, the TABASGO Foundation, and the Miller Institute for Basic Research in Science (U.C. Berkeley). A.M. acknowledges the financial support of the Brazilian funding agency FAPESP (Postdoc fellowship, process number 2014/11806-9). O.G. is supported by an NSF Astronomy and Astrophysics Postdoctoral Fellowship under award AST-1602595. J.H. was supported by a VILLUM FONDEN Investigator grant (project number 16599). S.J. was supported by JPL RSAs 143563, 1448524, 1460278, and 1473597.

Facilities: HST (WFC3)

REFERENCES

- Ade, P. A. R., et al. 2016, *Astron. Astrophys.*, 594, A13
 Alam, S., et al. 2016, Submitted to: *Mon. Not. Roy. Astron. Soc.*
 Andersen, P., & Hjorth, J. 2017
 Arnett, W. D. 1969, *ApJ*, 157, 1369
 Arnett, W. D., Branch, D., & Wheeler, J. C. 1985, *Nature*, 314, 337
 Avgoustidis, A., Verde, L., & Jimenez, R. 2009, *JCAP*, 0906, 012
 Betoule, M., Kessler, R., Guy, J., et al. 2014, *A&A*, 568, A22
 Bloom, J. S., et al. 2012, *Astrophys. J.*, 744, L17
 Chevallier, M., & Polarski, D. 2001, *Int. J. Mod. Phys.*, D10, 213
 Colgate, S. A., & McKee, C. 1969, *ApJ*, 157, 623
 Conley, A., Guy, J., Sullivan, M., et al. 2011, *ApJS*, 192, 1
 Daly, R. A., & Djorgovski, S. G. 2003, *Astrophys. J.*, 597, 9
 —. 2004, *Astrophys. J.*, 612, 652
 Dawson, K. S., Aldering, G., Amanullah, R., et al. 2009, *AJ*, 138, 1271
 Dickinson, M., Papovich, C., & Ferguson, H. C. 2001, in *Deep Fields*, ed. S. Cristiani, A. Renzini, & R. E. Williams, 68
 Frederiksen, T. F., Hjorth, J., Maund, J. R., et al. 2012, *Astrophys. J.*, 760, 125
 Giavalisco, M., Ferguson, H. C., Koekemoer, A. M., et al. 2004, *ApJ*, 600, L93
 Gilliland, R. L., Nugent, P. E., & Phillips, M. M. 1999, *ApJ*, 521, 30
 Graur, O., Rodney, S. A., Maoz, D., et al. 2014, *ApJ*, 783, 28
 Grogan, N. A., Kocevski, D. D., Faber, S. M., et al. 2011, *ApJS*, 197, 35
 Guy, J., et al. 2007, *Astron. Astrophys.*, 466, 11
 Hicken, M., Challis, P., Jha, S., et al. 2009, *ApJ*, 700, 331
 Hounsell, R., et al. 2017
 Hoyle, F., & Fowler, W. A. 1960, *Astrophys. J.*, 132, 565, [Erratum: *Astrophys. J.* 134, 1028 (1961)]
 Ishida, E. E. O., & de Souza, R. S. 2011, *Astron. Astrophys.*, 527, A49
 Jones, D. O., Rodney, S. A., Riess, A. G., et al. 2013, *ApJ*, 768, 166
 Jönsson, J., Dahlén, T., Goobar, A., et al. 2006, *ApJ*, 639, 991
 Jönsson, J., Sullivan, M., Hook, I., et al. 2010, *MNRAS*, 405, 535
 Kahaner, D., Moler, C., & Nash, S. 1988, *Numerical Methods and Software* (Upper Saddle River, NJ: Prentice Hall)
 Kessler, R., & Scolnic, D. 2017, *Astrophys. J.*, 836, 56
 Kessler, R., Becker, A. C., Cinabro, D., et al. 2009, *ApJS*, 185, 32
 Koekemoer, A. M., Faber, S. M., Ferguson, H. C., et al. 2011, *ApJS*, 197, 36
 Li, W., et al. 2011, *Nature*, 480, 348
 Linder, E. V. 2003, *Phys. Rev. Lett.*, 90, 091301
 Mortonson, M. J., Hu, W., & Huterer, D. 2009, *Phys. Rev.*, D79, 023004
 —. 2010, *Phys. Rev.*, D81, 063007
 Mortsell, E., & Clarkson, C. 2009, *JCAP*, 0901, 044
 Nielsen, J. T., Guffanti, A., & Sarkar, S. 2016, *Sci. Rep.*, 6, 35596
 Nomoto, K., Thielemann, F. K., & Yokoi, K. 1984, *Astrophys. J.*, 286, 644
 Nugent, P. E., et al. 2011, *Nature*, 480, 344
 Postman, M., Coe, D., Benítez, N., et al. 2012, *ApJS*, 199, 25
 Rest, A., Scolnic, D., Foley, R. J., et al. 2014, *ApJ*, 795, 44
 Riess, A. G., & Livio, M. 2006, *Astrophys. J.*, 648, 884
 Riess, A. G., Press, W. H., & Kirshner, R. P. 1996, *ApJ*, 473, 88
 Riess, A. G., Nugent, P. E., Gilliland, R. L., et al. 2001, *ApJ*, 560, 49
 Riess, A. G., Strolger, L.-G., Tonry, J., et al. 2004, *ApJ*, 607, 665
 Riess, A. G., Strolger, L.-G., Casertano, S., et al. 2007, *ApJ*, 659, 98
 Riess, A. G., et al. 2016, *Astrophys. J.*, 826, 56
 Rodney, S. A., Riess, A. G., Dahlen, T., et al. 2012, *ApJ*, 746, 5
 Rodney, S. A., Riess, A. G., Strolger, L.-G., et al. 2014, *AJ*, 148, 13
 Rodney, S. A., Riess, A. G., Scolnic, D. M., et al. 2015, *AJ*, 150, 156
 Rubin, D., Knop, R. A., Rykoff, E., et al. 2013, *ApJ*, 763, 35
 Sahni, V., & Starobinsky, A. 2006, *Int. J. Mod. Phys.*, D15, 2105
 Scolnic, D., & Kessler, R. 2016, *Astrophys. J.*, 822, L35
 Scolnic, D., et al. 2014, *Astrophys. J.*, 795, 45
 —. 2015, *Astrophys. J.*, 815, 117
 Scolnic, D. M., et al. 2017
 Shafer, D. L., et al. 2017
 Shafieloo, A. 2007, *Mon. Not. Roy. Astron. Soc.*, 380, 1573
 Shafieloo, A., Alam, U., Sahni, V., & Starobinsky, A. A. 2006, *Mon. Not. Roy. Astron. Soc.*, 366, 1081
 Shafieloo, A., & Clarkson, C. 2010, *Phys. Rev.*, D81, 083537
 Spergel, D., et al. 2015
 Stritzinger, M. D., Phillips, M. M., Boldt, L. N., et al. 2011, *AJ*, 142, 156
 Strolger, L.-G., Riess, A. G., Dahlen, T., et al. 2004, *ApJ*, 613, 200
 Suzuki, N., Rubin, D., Lidman, C., et al. 2012, *ApJ*, 746, 85
 Tegmark, M. 2002, *Phys. Rev.*, D66, 103507
 Tutusaus, I., Lamine, B., Dupays, A., & Blanchard, A. 2017, *Astron. Astrophys.*, 602, A73
 Wang, Y., & Tegmark, M. 2005, *Phys. Rev.*, D71, 103513